Band structures in doubly odd ^{98}Rh

S. Kumar,[1] S. Sihotra,[*] K. Singh,[†] V. Singh, Sandeep, J. Goswamy, N. Singh, and D. Mehta
Department of Physics, Panjab University, Chandigarh 160014, India

S. S. Malik
Department of Physics, Guru Nanak Dev University, Amritsar 143005, India

R. Palit
Department of Nuclear and Atomic Physics, Tata Institute of Fundamental Research, Mumbai 400005, India

R. Kumar, R. P. Singh, S. Muralithar, and R. K. Bhowmik
Inter-University Accelerator Centre, New Delhi 110067, India

(Received 24 December 2013; published 6 March 2014)

Excited states in the transitional doubly odd ^{98}Rh nucleus were populated in the ^{75}As(^{28}Si,$2p3n$) fusion-evaporation reaction using the 120-MeV incident ^{28}Si beam. The subsequent de-excitations were investigated through in-beam γ-ray spectroscopic techniques using an early implementation phase of the Indian National Gamma Array (INGA) spectrometer equipped with 18 clover Ge detectors. The level structures in ^{98}Rh have been established up to excitation energy $\approx$10 MeV and angular momentum $\sim 23\hbar$. The previously reported level schemes are considerably modified and extended substantially. Significant expansion of the level scheme at low excitation energies stipulates that the previously reported 842-726-994-980-265 keV γ-transition cascade in ^{98}Rh is not directly based on the ground state ($T_{1/2} = 8.7$ min). Tilted-axis cranking (TAC) shell-model calculations have been used to put the present level scheme of ^{98}Rh in perspective. Level structures have been interpreted in terms of the rotational bands based on the $\pi p_{1/2} \otimes \nu h_{11/2}$ [triaxiality parameter (γ) = 25°], and $\pi f_{5/2} \otimes \nu h_{11/2}$ proton-neutron configurations having moderate quadrupole deformation ($\epsilon_2 \approx 0.13$) and the admixtures. Excited band structures are based on the $\pi p_{1/2}/f_{5/2} \otimes \pi(g_{9/2})^2 \otimes \nu h_{11/2}$ configuration and the fully stretched $[\pi p_{1/2} \otimes \nu(h_{11/2})^2 \otimes \nu d_{5/2}]_{13^-}$ configuration.

DOI: 10.1103/PhysRevC.89.034303 PACS number(s): 21.10.−k, 21.60.−n, 23.20.−g, 27.60.+j

I. INTRODUCTION

Theoretical interpretation of the observed band structures in the doubly odd nuclei is far more involved as compared to the odd-A or even-even neighboring nuclei. It requires understanding of different types of coupling mechanisms of the odd-neutron and the odd-proton to the even-even core, and the Coriolis response of the neutron and proton motion to the rotation of the core, and proton-neutron ($\pi\nu$) residual interaction apart from various deformation-generating mechanisms for the even-even core. The coupling mode of an individual proton or neutron depends mainly on the deformation value of the core, the subshell angular momentum j, and its component Ω on the symmetry axis of the core. In the case of the doubly odd nuclei in the mass region $A \approx 80$, 105, 130, 160, and 190, the observed band structures based on the specific configurations involving valence quasiparticles in opposite shape-driving orbitals have resulted in systematics of various intriguing phenomena, viz., signature inversion and anomalous signature splitting [1–3], chiral twin bands [4], and recently predicted chopsticks-like motion of two angular momenta of the valence neutron and proton [5]. Interpretations of these phenomena have been fruitful theoretical construals over the years.

The odd-odd Rh ($Z = 45$) isotopes in the $A \approx 100$ mass region contain five protons in the $p_{1/2}$, $f_{5/2}$, and $g_{9/2}$ shells and the valence neutrons in the $d_{5/2}$, $g_{7/2}$, and $h_{11/2}$ shells outside the doubly quasimagic $^{90}_{40}$Zr core. Low-lying yrast states of the even-even $_{44}$Ru cores of the Rh isotopes are good examples of transitional systems between spherical vibrator and γ-soft nuclei [6–11]. The neighboring even-even nuclei, viz., ^{102}Ru and ^{106}Pd, exhibit the nonaxial vibrational modes usually known as quasi-γ bands [7,8], and the staggering signature parameters for these bands indicate the nuclei in this mass region to be γ soft. The doubly odd transitional nuclei do not exhibit well-developed rotational bands due to weakly deformed ($\beta_2 \sim 0.1$) γ-soft even-even cores. The proton and neutron Nilsson configuration assignments to the observed bands on the basis of observables, viz., $B(M1)/B(E2)$ ratios, band-crossing frequencies, and principle of coupling of alignment of the quasiproton and quasineutron bands in the neighboring odd-A nuclei, are quite challenging. Recent efforts in this mass region have resulted in the $\pi g_{9/2} \otimes \nu h_{11/2}$ bands exhibiting features of spontaneous breaking of chiral symmetry for the doubly odd ^{98,100}Tc [12,13] and ^{104,106}Rh [14,15] nuclei. Signature inversion phenomenon reported in the $\pi g_{9/2} \otimes \nu h_{11/2}$ bands in the doubly odd $^{98-102}$Rh and ^{104,106}Ag nuclei has been qualitatively understood as a competition between the Coriolis and $\pi\nu$ interactions [2] in a

[*] ssihotra@pu.ac.in
[†] Present address: Department of Applied Sciences, Chitkara University, Rajpura 140401, Punjab, India.

triaxial nucleus. The features related to triaxiality need to be explored for the lighter odd-odd Rh isotopes, where the $\nu h_{11/2}$ orbital is available at increasing excitation energies. The fully aligned terminating states of basic configurations obtained by coupling of limited valence quasiparticles outside the $^{90}_{40}$Zr core are expected to be in the medium spin region $\sim 20\hbar$ and are likely to compete energetically with the deformed collective structures in the experimentally observable spin region. The terminating states have been observed recently in the ^{98,99,100}Ru [10], ^{99,101,102}Rh [16–18], ^{98,99,102,103}Pd [19–22], and ^{98,99}Ag [23,24] nuclei and interpreted in terms of the valence-space and core-excited configurations using the cranked Nilsson-Strutinsky formalism [25].

As a part of the investigation to look for the abovementioned features, the detailed spectroscopy of the odd-odd ^{98}Rh ($N = 53$) nucleus is studied in the present work. Low-spin excited states in ^{98}Rh have been previously investigated from the β^+ and EC decay of ^{98}Pd ($T_{1/2} = 17.7$ min) [26,27], and the in-beam light-ion-induced ^{98}Ru(p,$n\gamma$) [28], ^{99}Ru(d,$3n$), and ^{96}Ru(α,np) [29] reactions. Concurrent γ-ray spectroscopic studies by Ghugre *et al.* [30] and Chattopadhyay *et al.* [31] using the heavy-ion-induced ^{65}Cu(^{36}S,$3n$) and ^{70}Ge(^{32}S,$3pn$) reactions have resulted in level scheme of ^{98}Rh up to high spins $\sim 20\hbar$. These investigations in ^{98}Rh have been performed using small detector arrays of Compton-suppressed Ge detectors. The results reported from the two experiments differ considerably. The present work reports the level scheme of the ^{98}Rh nucleus populated in heavy-ion-induced reaction and studied through the in-beam γ-ray spectroscopic techniques using a powerful γ-ray spectrometer [32] consisting of clover Ge detectors. The observed band structures are interpreted in the framework of tilted-axis cranking (TAC) shell-model [33] calculations. The investigations extend the present knowledge of the structure of ^{98}Rh. Preliminary reports on the present studies in the ^{98}Rh nucleus have been presented earlier [34,35].

II. EXPERIMENTAL DETAILS

Excited states in the ^{98}Rh nucleus were populated in the ^{75}As(^{28}Si,$2p3n$) fusion-evaporation reaction using the 120-MeV ^{28}Si beam. The experiment was carried out at the Inter-University Accelerator Centre (IUAC), New Delhi, and the ^{28}Si projectiles were provided by the 15UD Pelletron accelerator [36,37]. The target (thickness ~ 3 mg/cm^2) was prepared by vacuum evaporation of ^{75}As on to natural Pb backing (~ 10 mg/cm^2) followed by rolling. The ^{103}Ag compound nucleus produced in the present reaction is found to decay via several reaction channels associated with the (i) 5-particle emission, viz., $p4n$ (^{98}Pd) and $2p3n$ (^{98}Rh) with relative populations of $\sim 3\%$ and 10%, respectively, (ii) 4-particle emission, viz., $p3n$ (^{99}Pd), $2p2n$ (^{99}Rh), and $\alpha p2n$ (^{96}Ru), $2\alpha 2n$ (^{93}Tc) with relative populations of $\sim 8\%$, 22%, 16%, and 10% respectively, and (iii) 3-particle emission, viz., $p2n$ (^{100}Pd) and $\alpha 2n$ (^{97}Rh) with relative population of $\sim 7\%$ and 4%, respectively. The recoiled nuclei were stopped within the backed target. The γ-ray de-excitations have been investigated using an early implementation phase of the Indian National Gamma Array (INGA) comprising 18 large clover detectors mounted in five rings configuration [32]. The clover detectors used in the addback mode resulted in enhanced efficiency for high energy γ rays above ~ 1 MeV. The photopeak efficiency of INGA is $\sim 5\%$ at the 1.3-MeV γ-ray energy with all the 24 clover detectors in place. The energy and efficiency calibrations of the detectors were done using the ^{133}Ba and ^{152}Eu radioactive sources. Efficiency values at the higher energies up to ~ 3 MeV were deduced from the intensity balance along the transition sequences observed in the coincidence spectra with gate on the higher-lying transitions following de-excitations in the ^{38}Ar [38], ^{39}K [39], ^{93}Tc [40], and ^{96}Ru [9] nuclei. The ^{38}Ar and ^{39}K were produced as fission products in the reaction of ^{28}Si ion beam with the light nuclei present in the target, viz., the ^{27}Al frame of the target and ^{16}O in the oxide form. The ^{93}Tc and ^{96}Ru were produced in the 4-particle emission channels of the present fusion-evaporation reaction.

A total of about 300 million triple or higher-fold coincidence events were recorded for the γ rays emitted in the ^{75}As(^{28}Si,xpyn) fusion-evaporation reaction. The coincidence events were sorted in the offline analysis using INGASORT program [41] to produce symmetric E_γ-E_γ matrices and E_γ-E_γ-E_γ cubes in the Radford format. The RADWARE software package [42] was used to analyze the matrices and cubes. The available generalized background subtraction procedures were used for extracting single- and double-gated coincidence spectra, respectively. The γ-ray energy, intensity, and coincidence relationships for various observed transitions have been used to establish level scheme. The present level scheme of the ^{98}Rh nucleus is shown in Fig. 1. About 90 new transitions have been observed and placed in the level scheme. The representative coincidence spectra showing transitions in ^{98}Rh are shown in Figs. 2–4. The selectivity achieved by "double gating" and the presence of many crossover transitions in the level scheme of ^{98}Rh provide many checks on the placement and ordering of transitions and serve to augment confidence in the correctness of the proposed level scheme. Relative intensities of the γ rays emitted from the populated ^{98}Rh nucleus have been extracted from the singles spectra and the γ-γ coincidence spectra. The observation of weak γ transitions with relative intensity $\lesssim 10^{-3}$ as compared to the most intense transition was possible due to high statistics data collection. Improved sensitivity was achievable because of larger fraction of the higher-fold γ-ray coincidence events collected using INGA and use of clover detectors in the addback mode. Table I lists all the γ rays assigned to ^{98}Rh along with the intensities and proposed placements in the present level scheme (Fig. 1). The measured energies are accurate to 0.3 keV for intense γ rays. The errors increase up to 0.7 keV for weak and high-energy γ rays. The relative intensity values bear errors $\sim 5\%$ for γ rays below 1 MeV, which increase up to $\sim 10\%$ for the higher-energy γ rays and the low-lying γ rays feeding the isomeric states. The errors further increase up to $\sim 20\%$ for weak γ rays.

The multipolarity assignments to the γ transitions and spin-parity assignments to the excited nuclear states have been deduced mainly from the γ-ray angular distribution and polarization measurements. The directional correlation of oriented states (DCO) ratio analysis [43] has been used to identify the dipole (D) and the quadrupole (Q) transitions. Two dimensional angular correlation matrices between the

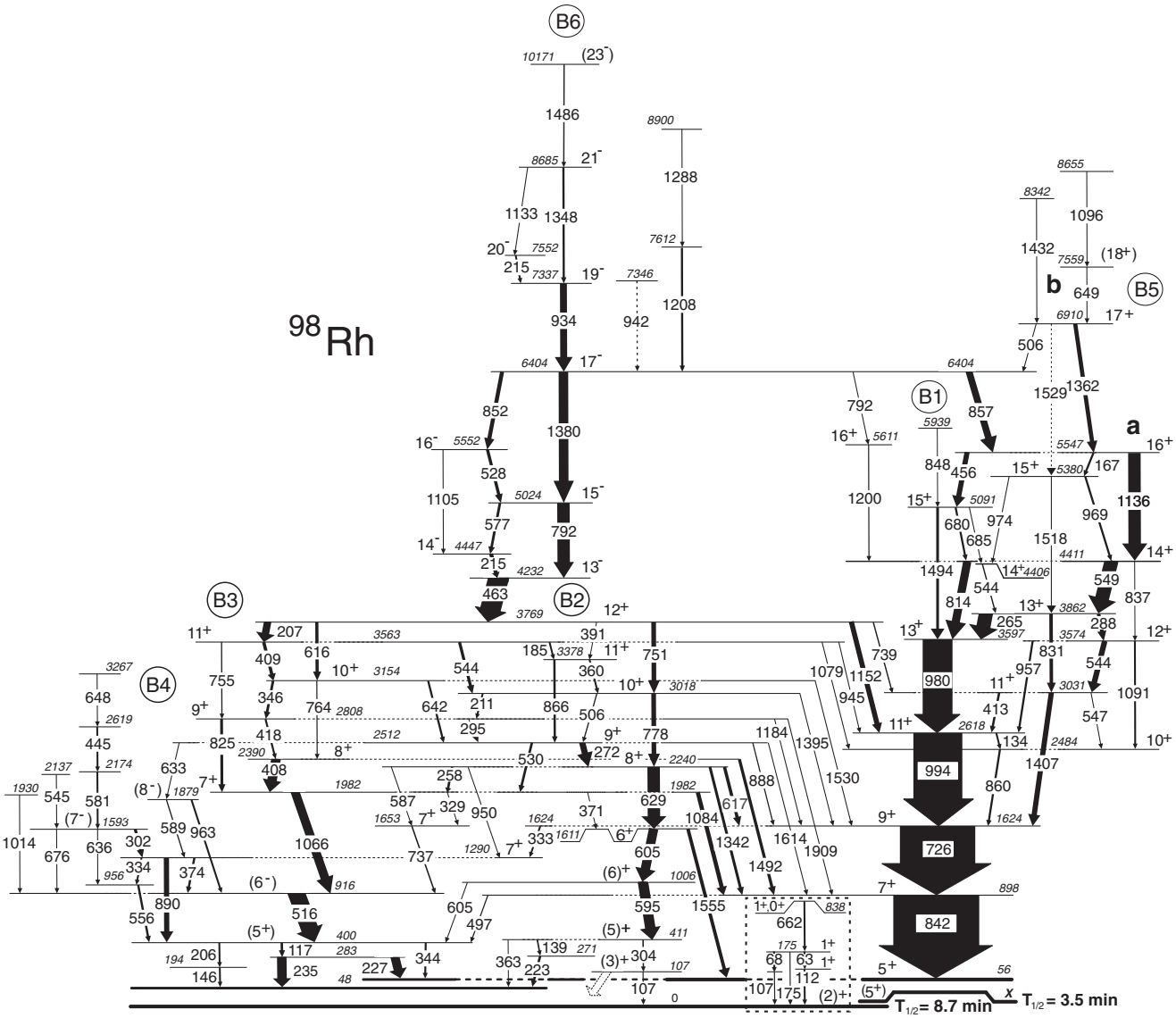

FIG. 1. Level scheme of ^{98}Rh obtained from the present work. Inset (dotted line) shows low-spin part established from the decay of ^{98}Pd [27]. Energies of γ rays and levels are given in keV. The width of the arrow representing the γ transition indicates relative intensity of the γ ray. Isomeric states are shown with thick horizontal lines. Excitation energy of the 3.5-min isomer is not known.

detectors at 90°, and those at 32° and 148° were constructed. Intensities of coincident transitions were mainly obtained from the correlation matrices by setting gates on the known low-lying stretched electric quadrupole ($E2$) transitions, viz., 842 keV ($7^+ \rightarrow 5^+$), 726 keV ($9^+ \rightarrow 7^+$), and 994 keV ($11^+ \rightarrow 9^+$) $E2$ transitions (Fig. 1) and used to deduce the DCO ratios. Other intense transitions, viz., 463 keV ($13^- \rightarrow 12^+$) identified to be dipole in the present work, are also used for the purpose wherever required. For the INGA geometry, the expected value of the DCO ratio is typically $\geqslant$1.0 for the quadrupole transition and $\leqslant$0.6 for the dipole transition with gate on the stretched $E2$ transition. DCO ratio values ~1 are, however, also expected for pure $\Delta I = 0$ dipole transitions [10]. To determine the electric or magnetic nature of the γ rays, the measurements were performed using the clover detectors at 90° as Compton polarimeter. The integrated polarization directional correlation from oriented nuclei (IPDCO) analysis [44] was performed using two asymmetric polarization matrices corresponding to the parallel and perpendicular segments (with respect to the emission plane) of the clover detector chosen as a Compton polarimeter along one axis and the coincident γ rays in all the detectors along the other axis. The DCO and IPDCO ratio values along with the assigned multipolarities for various transitions are also included in Table I.

III. RESULTS

A. Level scheme of ^{98}Rh

The level scheme of ^{98}Rh (Fig. 1) obtained from the present experiment consists of bands labeled B1–B6. The level scheme has been established up to spin ~23$\hbar$ and excitation energy ~10 MeV. It is a two-dimensional extension with considerable

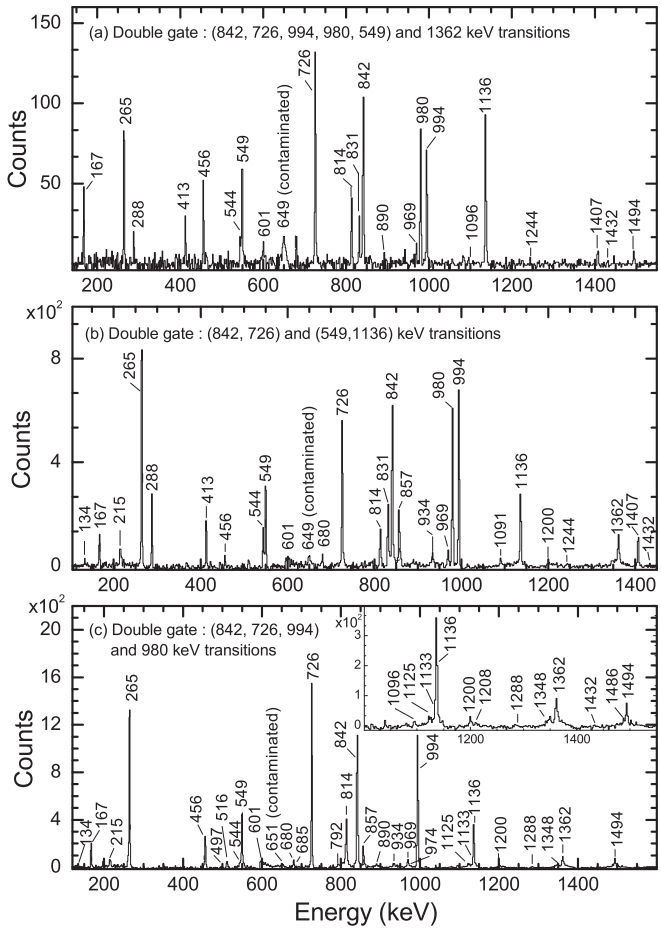

FIG. 2. The double-gated γ-ray coincidence spectra showing the transitions of bands B1 and B5. The spectra are generated with double coincidence gate on (a) one γ ray from the list of the 842-, 726-, 994-, 980-, and 549-keV γ rays, and the 1362-keV γ ray, (b) one γ ray from the list of the 842- and 726-keV γ rays, and the other from the list of the 549- and 1136-keV γ rays, and (c) one γ ray from the list of the 842-, 726-, and 994-keV γ rays, and the 980-keV γ ray.

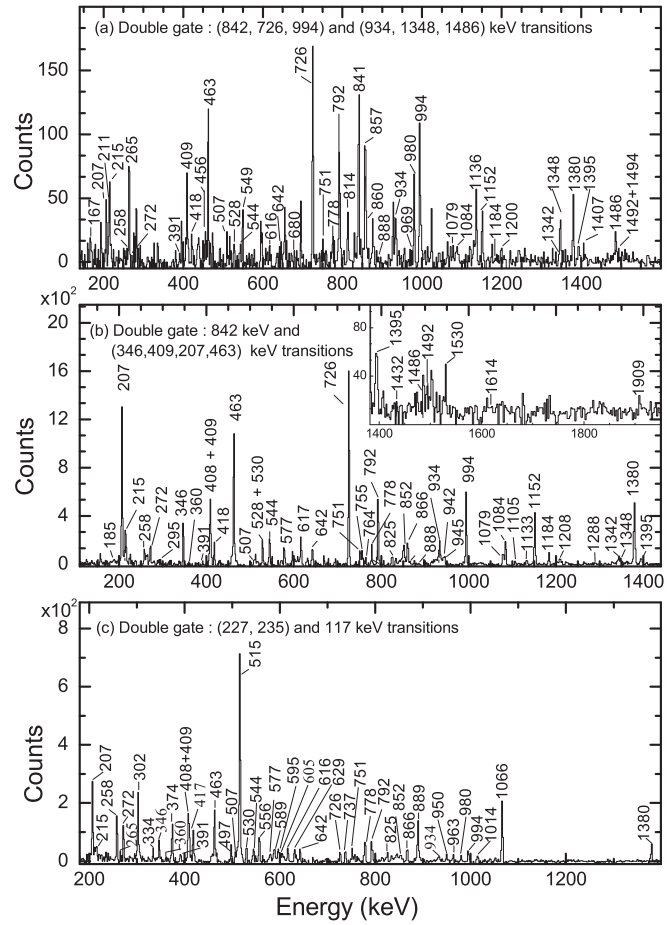

FIG. 3. The double-gated γ-ray coincidence spectra showing the transitions of bands B1, B2, B3, B4, and B6. The spectra are generated with double coincidence gate on (a) one γ ray from the list of the 842-, 726-, and 994-keV γ rays and the other from the list of the 934-, 1348-, and 1486-keV γ rays, and (b) the 842-keV γ ray and the other from the list of the 346-, 409-, 207-, and 463-keV γ rays, and (c) one γ ray from the list of the 227- and 235-keV γ rays and the 117-keV γ ray.

modification of the earlier reported level schemes [30,31]. The investigations from the β^+ and EC radioactive decay spectroscopy of ^{98}Rh [45] have led to identification of the ground state with $T_{1/2} = 8.7$ min and an isomeric state with $T_{1/2} = 3.5$ min. Banerjee *et al.* [46] have assigned $I^\pi = 2^+$ for the ground state ($T_{1/2} = 8.7$ min) of ^{98}Rh on the basis that it undergoes β decay only to the 2^+ state of the even-even ^{98}Ru nucleus, and there is no direct β feeding to either the 4^+ excited state or the 0^+ ground state. The excitation energy of the isomeric state with $T_{1/2} = 3.5$ min is not known. It decays predominantly to the ground state of ^{98}Rh by the isomeric transition (IT) with a total branching of ~89%, and the excited states of ^{98}Ru by the β^+ and EC decay with branching of ~11% [27]. The isomeric state has been assigned $I^\pi = (5^+)$ on the basis of the allowed β decay to the 4^+ and 6^+ states in ^{98}Ru [27]. Due to large difference in the spin values, the ground state and the isomeric state in ^{98}Rh undergo β^+ and EC decay mainly to the mutually exclusive sets of states in ^{98}Ru. Various low-lying states of ^{98}Rh have been identified in the β^+ and EC decay from the 0^+ ground state of the ^{98}Pd nucleus ($T_{1/2} = 17.7$ min) [27]. The low-lying states of ^{98}Rh populated in the decay that are relevant to the present work are shown as inset in the Fig. 1. The (5^+) isomeric state of ^{98}Rh with $T_{1/2} = 3.5$ min is not populated in this decay.

The 842-726-994-980-265 keV γ-transition cascade has been assigned to the ^{98}Rh nucleus on the basis of excitation function studies of the ^{96}Ru(α,np) and ^{99}Ru(d,3n) reactions by Behar *et al.* [29]. Further, on the basis of investigations of the intensity balance between the prompt and activity decay deduced from these α-particle- and deuteron-induced reactions with alternate on-off beam experiments, it has been concluded that this γ-transition cascade is based on the (2^+) ground state ($T_{1/2} = 8.7$ min). Later, contemporaneous investigations by Ghugre *et al.* [30] and Chattopadhyay *et al.* [31] using the ^{65}Cu(^{36}S,3n) and ^{70}Ge(^{32}S,3pn) fusion-evaporation reactions, respectively, have resulted in the level scheme of ^{98}Rh up to excitation energy ~10 MeV. Both the groups have considered

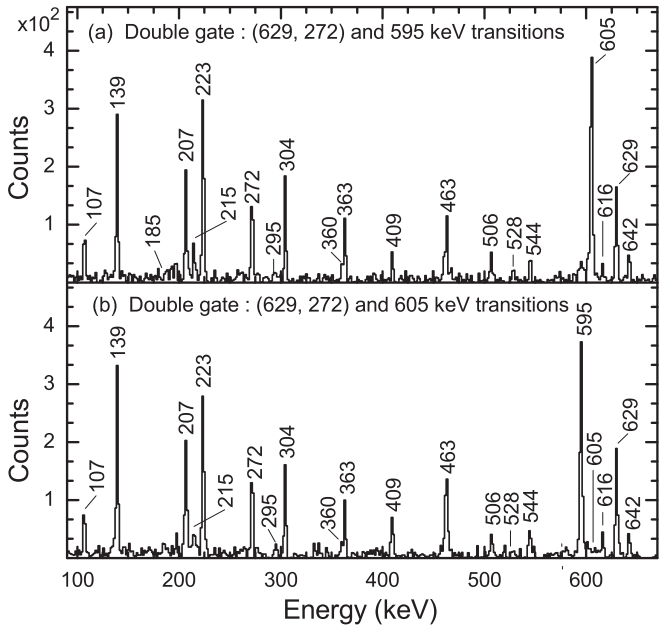

FIG. 4. The double-gated γ-ray coincidence spectrum showing the transitions of bands B2, B3, and B6. The spectrum is generated with double coincidence gate on one of the 629- and 272-keV γ rays, with (a) the 595-keV γ ray and (b) the 605-keV γ ray.

the 842-726-994-980-265 keV γ-transition cascade to be based on the (2^+) ground state as proposed by Behar *et al*. [29]. The level schemes reported from the previous investigations [30,31] in ^{98}Rh are found to differ considerably both in terms of the placement of the γ transitions and the multipolarity assignments. The present level scheme shown in Fig. 1 preserves the general features based on the γ-ray coincidence relationships in the previous established schemes [30,31], which show mainly the γ transitions involved in the bands B1, B5, and B6 (Fig. 1).

The 792-1380-934-1348-1486 keV γ-transition sequence (band B6) is reported to feed the 11^+ state (Fig. 1) in band B1 via the 463 ($M1$)–215 ($E1$) keV transition cascade by Ghugre *et al*. [30], and only the 463 keV ($M1$) dipole transition by Chattopadhyay *et al*. [31]. The previously reported 209- and 215-keV transitions [30] placed above and in the decay, respectively, of this sequence are not observed in the present work. The 577-215 keV and 1133-215 keV dipole cascades are observed to form the coupled structure with the 792-keV and 1348-keV $E2$ crossover transitions lying in this sequence. Another energetically feasible 215-keV transition depopulating the 271-keV state to the 56-keV isomeric state (Fig. 1) is not seen. Ghugre *et al*. [30] have reported two different 934-keV transitions present in the 463-792-1380-934-1348 keV (band B6) and 1136-1364-857-934 keV (band B1) cascades. In the present work, a single 934-keV transition $19^- \rightarrow 17^-$ is observed in band B6 and the 17^- state decays to the two 16^+ states at 5547 (band B5) and 5611 keV through the 857- and 792-keV transitions, respectively. A 1152-keV transition has been reported by Ghugre *et al*. [30] in parallel to the 1486-keV transition in band B6. In the present

TABLE I. The γ-ray energies (E_γ), de-exiciting level energies (E_i), relative intensities, spin assignments, DCO and IPDCO ratios, and multiploarity assignments for the transitions in ^{98}Rh. The DCO ratios are obtained from the gated spectra on the stretched electric quadrupole ($E2$) transitions, as mentioned in the text. Errors associated with the IPDCO values range 10–25%.

E_γ (keV)	E_i (keV)	Intensity	Spin assignment $(I_i^\pi \rightarrow I_f^\pi)$	DCO	IPDCO	Multipolarity assignment
106.8	107	3.0(6)	$(3)^+ \rightarrow (2)^+$			($M1$)
117.0	400	29(4)	$(5^+) \rightarrow$	0.92(18)		Q
134.0	2618	7.0(9)	$11^+ \rightarrow 10^+$			$M1$
138.9	411	18.0(25)	$(5)^+ \rightarrow$			
145.6	194	2.7(6)				
167.3	5547	24(2)	$16^+ \rightarrow 15^+$	0.53(7)		$M1$
184.6	3563	7.3(8)	$11^+ \rightarrow 11^+$			
206.5	400	3.5(5)	$(5^+) \rightarrow$			
206.5	3769	86(6)	$12^+ \rightarrow 11^+$	0.59(6)	−0.09(3)	$M1$
210.9	3018	1.6(2)	$10^+ \rightarrow 9^+$			$M1$
215.1	4447	45(3)	$14^- \rightarrow 13^-$			$M1$
215.2	7552	15.0(15)	$20^- \rightarrow 19^-$			$M1$
223.4	271	28(2)				
227.3	283	104(10)	$\rightarrow 5^+$	0.45(9)		D
235.1	283	111(10)		0.92(18)		Q
258.3	2240	28(3)	$8^+ \rightarrow 7^+$	0.44(8)		$M1$
264.8	3862	164(10)	$13^+ \rightarrow 13^+$	0.85(8)	−0.03(1)	D
271.6	2512	72(6)	$9^+ \rightarrow 8^+$			$M1$
287.9	3862	41(5)	$13^+ \rightarrow 12^+$	0.56(10)		$M1$
295.5	2808	7.7(11)	$9^+ \rightarrow 9^+$			
302.4	1593	34(3)	$(7^-) \rightarrow 7^+$			
304.1	411	16.0(20)	$(5)^+ \rightarrow (3)^+$			
329.0	1982	9.1(15)	$7^+ \rightarrow 7^+$			

TABLE I. (*Continued.*)

E_γ (keV)	E_i (keV)	Intensity	Spin assignment $(I_i^\pi \rightarrow I_f^\pi)$	DCO	IPDCO	Multipolarity assignment
333.3	1624	12.0(20)	$9^+ \rightarrow 7^+$			$E2$
334.2	1290	7.7(14)	$7^+ \rightarrow$			
344.2	400	23.2(23)	$(5^+) \rightarrow 5^+$			
346.1	3154	30.0(24)	$10^+ \rightarrow 9^+$	0.55(6)		$M1$
359.6	3378	2.3(4)	$11^+ \rightarrow 10^+$			$M1$
362.6	411	7.5(12)	$(5)^+ \rightarrow$			
371.0	1982	10.5(15)	$7^+ \rightarrow 6^+$			$M1$
374.1	1290	26.0(2.6)	$7^+ \rightarrow (6^-)$			$(E1)$
391.4	3769	10.0(14)	$12^+ \rightarrow 11^+$			$M1$
407.6	2390	111(9)	$8^+ \rightarrow 7^+$	0.61(8)	−0.03(1)	$M1$
409.1	3563	38(4)	$11^+ \rightarrow 10^+$	0.40(6)		$M1$
413.0	3031	27(3)	$11^+ \rightarrow 11^+$	0.81(14)		
417.8	2808	23.0(2.5)	$9^+ \rightarrow 8^+$	0.64(11)		$M1$
445.0	2619	2.0(4)				
456.2	5547	60(5)	$16^+ \rightarrow 15^+$	0.45(6)	−0.04(2)	$M1$
462.7	4232	240(17)	$13^- \rightarrow 12^+$	0.51(5)	0.08(2)	$E1$
497.4	898	13.8(17)	$7^+ \rightarrow (5^+)$			$(E2)$
506.1	6910	1.6(3)	$17^+ \rightarrow 17^-$			$E1$
506.5	3018	14.2(14)	$10^+ \rightarrow 9^+$			$M1$
515.6	916	202(16)	$(6^-) \rightarrow (5^+)$	0.41(4)		$(E1)$
528.3	5552	36(3)	$16^- \rightarrow 15^-$	0.52(7)		$M1$
529.8	2512	29(3)	$9^+ \rightarrow 7^+$			$E2$
543.6	3574	66(5)	$12^+ \rightarrow 11^+$	0.59(6)	−0.02(1)	$M1$
544.0	4406	39(4)	$14^+ \rightarrow 13^+$	0.53(8)		$M1$
544.4	3563	35(4)	$11^+ \rightarrow 10^+$			$M1$
545.0	2137	4.1(6)	$\rightarrow (7^-)$			
547.2	3031	12.1(14)	$11^+ \rightarrow 10^+$			$M1$
548.9	4411	162(10)	$14^+ \rightarrow 13^+$	0.50(5)	−0.03(1)	$M1$
555.8	956	26(3)	$\rightarrow (5^+)$			
577.1	5024	30(3)	$15^- \rightarrow 14^-$	0.57(9)		$M1$
581.2	2174	8.2(10)	$\rightarrow (7^-)$			
587.1	2240	1.3(3)	$8^+ \rightarrow 7^+$			$M1$
589.3	1879	14.0(20)	$(8^-) \rightarrow 7^+$			$(E1)$
594.9	1006	126(10)	$(6)^+ \rightarrow (5)^+$	0.48(6)		$(M1)$
600.8		3.6(8)				
605.2	1611	114(9)	$6^+ \rightarrow (6)^+$	0.93(12)		
605.5	1006	2.8(6)	$(6)^+ \rightarrow (5^+)$			$(M1)$
615.8	3769	37(3)	$12^+ \rightarrow 10^+$			$E2$
616.8	2240	38(3)	$8^+ \rightarrow 9^+$			$M1$
629.4	2240	145(10)	$8^+ \rightarrow 6^+$	0.80(10)		$E2$
632.6	2512	6.6(8)	$9^+ \rightarrow (8^-)$			$(E1)$
636.2	1593	5.3(7)	$(7^-) \rightarrow$			
641.7	3154	25.0(22)	$10^+ \rightarrow 9^+$			$M1$
648.0	3267	0.80(16)				
649.2	7559	9.1(20)	$(18^+) \rightarrow 17^+$			$(M1)$
676.4	1593	5.5(8)	$(7^-) \rightarrow (6^-)$			$(M1)$
680.0	5091	24.3(20)	$15^+ \rightarrow 14^+$	0.51(7)		$M1$
685.0	5091	5.8(8)	$15^+ \rightarrow 14^+$			$M1$
725.6	1624	877(44)	$9^+ \rightarrow 7^+$	0.99(8)	0.10(2)	$E2$
737.0	1653	16.9(23)	$7^+ \rightarrow (6^-)$			$(E1)$
738.6	3769	20.0(21)	$12^+ \rightarrow 11^+$			$M1$
750.9	3769	54(5)	$12^+ \rightarrow 10^+$	0.77(12)		$E2$
755.4	3563	14.1(20)	$11^+ \rightarrow 9^+$			$E2$
764.1	3154	13.2(20)	$10^+ \rightarrow 8^+$	1.3(2)		$E2$
778.0	3018	54(5)	$10^+ \rightarrow 8^+$	0.71(10)		$E2$
792.0	5024	145(9)	$15^- \rightarrow 13^-$	0.97(10)	0.09(2)	$E2$
792.3	6404	12.0(20)	$17^- \rightarrow 16^+$			$E1$

TABLE I. (*Continued.*)

E_γ (keV)	E_i (keV)	Intensity	Spin assignment ($I_i^\pi \rightarrow I_f^\pi$)	DCO	IPDCO	Multipolarity assignment
813.9	4411	95(7)	$14^+ \rightarrow 13^+$	0.47(6)	−0.03(1)	$M1$
825.1	2808	33(5)	$9^+ \rightarrow 7^+$	1.08(24)		$E2$
831.5	3862	41(3)	$13^+ \rightarrow 11^+$	0.89(12)	0.05(2)	$E2$
836.6	4411	9.0(16)	$14^+ \rightarrow 12^+$			$E2$
841.6	898	1000(50)	$7^+ \rightarrow 5^+$	0.97(8)	0.10(2)	$E2$
848.0	5939		$\rightarrow 15^+$			
851.6	6404	47(5)	$17^- \rightarrow 16^-$	0.56(8)	−0.03(1)	$M1$
856.6	6404	81(7)	$17^- \rightarrow 16^+$	0.58(7)	0.03(1)	$E1$
860.2	2484	27(3)	$10^+ \rightarrow 9^+$	0.54(8)		$M1$
866.2	3378	26(3)	$11^+ \rightarrow 9^+$	0.96(15)		$E2$
888.4	2512	13.5(15)	$9^+ \rightarrow 9^+$			
889.6	1290	61(6)	$7^+ \rightarrow (5^+)$			$(E2)$
933.6	7337	81(7)	$19^- \rightarrow 17^-$	1.02(12)	0.05(2)	$E2$
942.0	7346	14.0(15)	$\rightarrow 17^-$			
945.3	3563	5.9(8)	$11^+ \rightarrow 11^+$			
950.1	2240	1.6(3)	$8^+ \rightarrow 7^+$			$M1$
956.6	3574	25(3)	$12^+ \rightarrow 11^+$	0.72(15)		$M1$
962.8	1879	22(3)	$(8^-) \rightarrow (6^-)$			$(E2)$
969.1	5380	26(3)	$15^+ \rightarrow 14^+$	0.40(9)		$M1$
973.8	5380	1.5(3)	$15^+ \rightarrow 14^+$			$M1$
979.7	3597	347(17)	$13^+ \rightarrow 11^+$	0.97(8)	0.08(2)	$E2$
994.0	2618	570(28)	$11^+ \rightarrow 9^+$	1.02(8)	0.06(2)	$E2$
1014.0	1930	15.9(19)	$\rightarrow (6^-)$			
1066.0	1982	103(7)	$7^+ \rightarrow (6^-)$	0.40(4)		$(E1)$
1079.2	3563	11.0(15)	$11^+ \rightarrow 10^+$			$M1$
1084.4	1982	50(4)	$7^+ \rightarrow 7^+$			
1090.6	3574	22(3)	$12^+ \rightarrow 10^+$	1.0(2)	0.02(1)	$E2$
1096.1	8655	5.7(14)				
1105.1	5552	8.9(13)	$16^- \rightarrow 14^-$			$E2$
1132.7	8685	11.2(16)	$21^- \rightarrow 20^-$			$M1$
1136		2.2(5)	$\rightarrow 16^+$			
1136.2	5547	145(9)	$16^+ \rightarrow 14^+$	0.94(9)	0.06(1)	$E2$
1151.7	3769	59(4)	$12^+ \rightarrow 11^+$	0.44(5)		$M1$
1183.7	2808	10.0(14)	$9^+ \rightarrow 9^+$			
1200.3	5611	16.6(20)	$16^+ \rightarrow 14^+$			$E2$
1208.0	7612	25(3)	$\rightarrow 17^-$	0.8(2)		
1244.2		3.0(6)				
1288.2	8900	10.0(15)				
1342.2	2240	35(4)	$8^+ \rightarrow 7^+$	0.50(9)		$M1$
1347.7	8685	27(3)	$21^- \rightarrow 19^-$	1.01(18)		$E2$
1361.9	6910	53(4)	$17^+ \rightarrow 16^+$	0.55(6)		$M1$
1379.7	6404	124(10)	$17^- \rightarrow 15^-$	0.83(14)	0.07(2)	$E2$
1394.9	3018	4.9(8)	$10^+ \rightarrow 9^+$			$M1$
1407.0	3031	70(5)	$11^+ \rightarrow 9^+$	0.97(9)	0.03(1)	$E2$
1432.2	8342	5.5(7)	$\rightarrow 17^+$			
1486.2	10171	17.7(26)	$(23^-) \rightarrow 21^-$			$(E2)$
1491.9	2390	42(4)	$8^+ \rightarrow 7^+$	0.56(7)		$M1$
1493.7	5091	37(3)	$15^+ \rightarrow 13^+$	0.87(14)	−0.03(1)	$E2$
1517.8	5380	13.2(19)	$15^+ \rightarrow 13^+$			$E2$
1529.0	6910	1.8(4)	$17^+ \rightarrow 15^+$			$E2$
1530.4	3154	5.4(10)	$10^+ \rightarrow 9^+$			$M1$
1554.6	1611	49(4)	$6^+ \rightarrow 5^+$	0.44(8)		$M1$
1614.1	2512	7.7(12)	$9^+ \rightarrow 7^+$			$E2$
1821		3.0(6)				
1836		2.5(6)				
1909.3	2808	1.3(3)	$9^+ \rightarrow 7^+$			$E2$
2064		2.8(6)				

level scheme, this transition is placed as de-exciting the 3769-keV level and feeding the 11^+ level at 2618 keV in band B1. The previously reported 1208-1288 keV cascade [30] feeding the 6404-keV state is confirmed. The 1436- and 1547-keV transitions placed parallel to this cascade by Ghugre *et al.* [30] are not observed.

The ordering of the transitions in the 456-1494 keV transition cascade reported by Ghugre *et al.* [30] as parallel to the 1136-549-265 keV cascade is reversed, which is well supported by the newly observed coupled structure of transitions. A weakly populated 4406-keV state with decay and feeding patterns similar to close-lying 4411-keV state of band B5 is also observed. The previously reported 1230- and 1312-keV transitions as crossover to the 680-549 keV and 456-857 keV [31] transition cascades, respectively, and the 1125-keV transition [30] above the 549-keV transition (band B5) are not observed in the present work [Figs. 2(b) and 2(c)]. The intensities of transitions above the 6910-keV state are significantly reduced as compared to the depopulating 1362-keV transition [Figs. 2(b) and 2(c)], indicating considerable multifragmentation above this level. The 601-, 649-, 1096-, 1244-, 1432-, 1821-, and 2064-keV weak γ rays [Fig. 2(a)] are observed above the 6910-keV level, and the 890-, 1136-, and 1611-keV weak γ rays are observed above the 4411-keV level. The placements of these transitions could not be ascertained in the present work. The 651-890-1096 keV transition cascade (Fig. 1) reported earlier [30] as feeding the level above the 1362-keV transition is not confirmed in the present work.

Ghugre *et al.* [30] have placed the cascade involving 207- and 409-keV transitions parallel to the 994-keV transition (band B1), i.e., depopulating the 2618-keV level and feeding the 1624-keV level (Fig. 1). This cascade is not reported by Chattopadhyay *et al.* [31]. In the present work, the 207- and 409-keV transitions are not observed in coincidence with the 980-keV transition [Figs. 2(b) and 2(c)]; rather these transitions are observed to depopulate the 3769-keV state fed by the 463-keV transition. The coincidence spectra with gates on the 207- and 409-keV transitions resulted in considerable extension of the level scheme in the lower excitation energy part. Three new coupled bands B2, B3, and B4 are established, which coexist with band B1. The relevant gated spectra are shown in Figs. 3 and 4. The states of bands B2 and B3 exhibit intense interband transitions and also decay to the 5^+, 7^+, 9^+, and 11^+ yrast states in band B1 through multiple transitions with $\Delta I = 0, 1, 2$ [Fig. 2(b)].

The lowest state in the present level scheme (Fig. 1) is observed in the decay of band B2 through the 629-605-595-304-107 keV transition cascade. Figures 4(a) and 4(b) show the coincidence spectra generated with double coincidence gate on one of the 629- and 272-keV γ rays, and (a) the 595-keV γ ray and (b) the 605-keV γ ray. The spectra show similar intensity patterns for the lower-lying transitions (Fig. 1). Intensity of the 107-keV transition relative to the 139-, 223-, and 304-keV transitions is found to be consistent in the coincidence spectra with gate on the higher-lying transitions. It supports the present placement of the 107-keV transition (Fig. 1). The intensity balance at the 411-keV state in the coincidence spectra with gates on the higher-lying 605- and 629-keV transitions is also reasonably satisfied; i.e., intensity of the 595-keV transition is balanced by sum of intensities of the 223-, 304-, and 363-keV decay transitions. The ordering of the 139- and 223-keV transitions could not be ascertained. It is worth mentioning that the 107-keV state has also been identified in ^{98}Rh in the conversion electron and γ-ray measurements [26,27] following its population in the β^+ and EC radioactive decay of ^{98}Pd ($T_{1/2} = 18$ min). The 107-keV transition has been assigned to be $M1$ on the basis of the measured total internal coefficient, $\alpha_T = 0.26(7)$ [26]. In the ^{98}Rh nucleus populated in the present fusion-evaporation reaction, it has been observed that the 107-keV γ-ray intensity accounts for less than 20% of the 304-keV γ-ray intensity in the coincidence spectra with gates on the higher-lying 595-, 605-, and 629-keV transitions. The observed intensity loss can be due to the unidentified low-energy transitions, internal conversion of 107-keV transition, or significant lifetime of the de-exciting state. Overall, it infers that the 107-keV state in ^{98}Rh populated in the fusion-evaporation reaction is likely to be different from the one observed in the decay of ^{98}Pd (Fig. 1).

It is proposed that the lowest observed state populated by the 107-keV transition is the ground state in ^{98}Rh. The extension of the present level scheme with this presumption implies that the 842-726-994-980-265 keV γ-transition cascade feeds a state at 56 keV. This state is also populated by the new 117-227 keV transition cascade along with the 344-keV crossover transition in the decay of band B3. The above-mentioned observations demand modifications in the previous level scheme [30,31] with the assignment of the 842-726-994-980-265 keV γ-transition cascade based on the 56-keV excited state rather than the ground state, as had been taken earlier [30,31]. The possibility that the 56-keV excited state is the same as the earlier observed (5^+) isomeric state ($T_{1/2} = 3.5$ min) with unestablished excitation energy [26,27] is not likely because it is in contradiction with the observations of Behar *et al.* [29] that the 842-keV transition populates the ground state with $T_{1/2} = 8.7$ min. The de-exciting transition from the 56-keV state to the ground state is not observed in the present measurements. It is proposed that the 842-keV transition populates an isomeric state at 56 keV with half-life much shorter than that of the ground state ($T_{1/2} = 8.7$ min) and considerably longer than the coincidence time window ($\sim 200\,ns$) used in the present work.

Another excited state at 48 keV is proposed in the present level scheme (Fig. 1), which is fed by (i) the 235-keV γ transition from the intermediate state of the 117-227 keV γ-transition cascade, (ii) the 206-146 keV γ-transition cascade in parallel to the 117-235 keV transition cascade, and the 139-223 keV transition cascade with the 363-keV crossover transition from the 411-keV state. The ordering of the 206-146 keV transition cascade is uncertain. In the coincidence spectra with gate on the higher-lying 408-, 463-, and 1066-keV transitions, the intensity of the 516-keV transition is reasonably balanced by the sum of intensities of the 146-, 235-, 227-, and 344-keV transitions. It is mentioned that the observed intensity of the 117-keV γ ray accounts for only $\sim$25% of the intensity feeding in the 400-keV level. The intensity loss can be due to internal conversion or an unidentified parallel transition cascade. The decay of the 48- and 56-keV states to the ground state could not be established

in the present work. Further experiments in this direction are warranted to study the isomeric decays.

B. Spin-parity assignments to states in ^{98}Rh

The spin-parity assignments to the observed states shown in the present level scheme of ^{98}Rh (Fig. 1) are tentative in view of the unestablished decay of the newly observed low-lying states to the ground state, and lack of information regarding multipolarity of the low-lying transitions from the present expeirment. An attempt has been made for relative spin-parity assignments on the basis of usual multipolarity for the decay transitions, DCO ratios, and limited polarization measurements. It is assumed that the multipolarities of these γ rays are in general not higher than quadrupole and that the quadrupoles are $E2$'s. It has been observed that in general, parity-changing transitions are highly retarded and cannot compete with the $M1$ or $E2$ transitions of comparable energy. Spin assignments have been mainly deduced from the presumptions that (a) a high-spin state decays predominantly to the state with lower spin through $J \rightarrow J\text{-}L$ transition of multipolarity L, (b) weak crossover transition to two dipole transitions in a coupled band is generally taken as $E2$ in case the DCO ratio is not known, and (c) the yrast states are preferentially populated following the heavy-ion reactions. In the odd-odd ^{98,100}Tc [12,13], ^{96,100,102,104}Rh [14,18,47–49], and ^{100,106,108}Ag [50–53] nuclei in the $A \approx 100$ mass region, the low-lying states with excitation energy up to $\sim$0.5 MeV are mainly positive-parity states with $I \leqslant 8\hbar$, which are built on the $\pi g_{9/2} \otimes \nu g_{7/2}/\nu d_{5/2}$ and $\pi p_{1/2} \otimes \nu h_{11/2}$ configurations. The low-lying negative-parity states are scarce in the odd-odd Tc, Rh, and Ag nuclei in the $A \approx 100$ region. The 2^- ground state of ^{102}Rh [18] based on the $\pi p_{1/2} \otimes \nu g_{7/2}/\nu d_{5/2}$ configuration has been observed. Low-lying states of the negative-parity band based on the $\pi g_{9/2} \otimes \nu h_{11/2}$ configuration are observed only in the heavier $^{104-112}$Rh [14,15,54] isotopes. The decoupled nature of band B1 favors the $\pi p_{1/2} \otimes \nu h_{11/2}$ configuration assignment. The detailed discussion in this regard is given later in Sec. IV. In view of these points, the spin-parity for the bandhead of band B1 at 56 keV is conjectured to be around 5^+. Taking $I^\pi = 5^+$ for the 56-keV state, the states in band B1 are assigned spin-parity values along the 842-726-994-980-1494 keV sequence consisting of the stretched $E2$ transitions. The present measured DCO ratio values for the 980- and 1494-keV transitions support these to be $E2$ [Figs. 5(b) and 5(c)] and the 5091-keV level is assigned $I^\pi = 15^+$. The present measured DCO [Fig. 5(a)] and IPDCO ratio values for the 1407-keV transition (Table I) support it being $E2$ as proposed by Ghugre *et al.* [30] and the 3031-keV level is assigned $I^\pi = 11^+$. It may be mentioned that the 980-, 1407-, and 1494-keV transitions were assigned to be $E1$, $E2$, and $E1$, respectively, by Ghugre *et al.* [30], and $E2$, $E1$, and $E1$, respectively, by Chattopadhyay *et al.* [31]. The DCO ratio value 0.89(12) for the 831-keV crossover transition indicate the quadrupole nature. The DCO ratios for the 288-, 549-, and 814-keV transitions support the dipole nature and have been assigned as $13^+ \rightarrow 12^+$, $14^+ \rightarrow 13^+$, and, $14^+ \rightarrow 13^+$, respectively. The 4411-keV level is assigned $I^\pi = 14^+$. The present DCO ratio value 0.85(8) for the 265-keV transition [Fig. 5(d)] correspond either to stretched quadrupole or $\Delta I = 0$ dipole character. The parallel cascades of the 994-980-265 keV transitions and the 1407-831 keV transitions are placed between the same 1624- and 3862-keV levels, and the measured DCO ratios $\sim$1 for all the transitions in the cascades support the 265-keV transition as $13^+ \rightarrow 13^+$

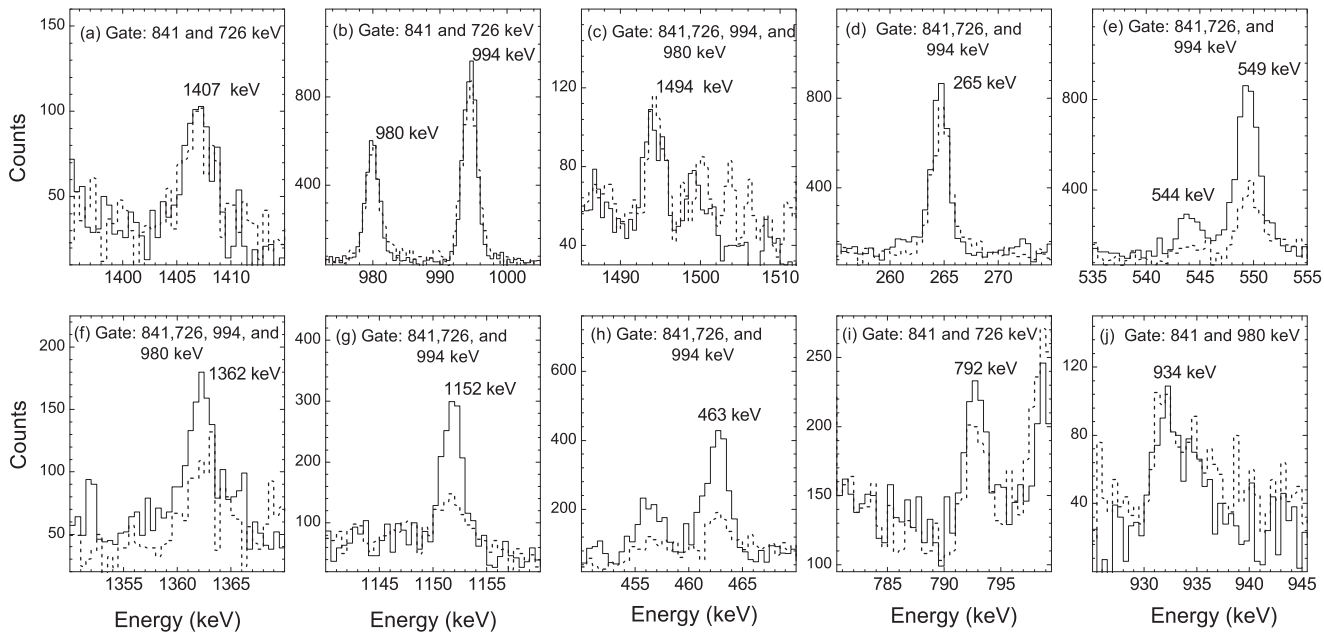

FIG. 5. The summed coincidence spectra generated to deduce DCO ratios for the (a) 1407 ($11^+ \rightarrow 9^+$), (b) 980 ($13^+ \rightarrow 11^+$) and 994 ($11^+ \rightarrow 9^+$), (c) 1494 ($15^+ \rightarrow 13^+$), (d) 265 ($13^+ \rightarrow 13^+$), (e) 549 ($14^+ \rightarrow 13^+$), (f) 1362 ($17^+ \rightarrow 16^+$), (g) 1152 ($12^+ \rightarrow 11^+$), (h) 463 ($13^- \rightarrow 12^+$), (i) 792 ($15^- \rightarrow 13^-$), and (j) 934 ($19^- \rightarrow 17^-$) keV γ transitions by setting gates on the lower-lying quadrupole transitions. The coincidence spectra obtained from the two angular correlation matrices are shown overlapping.

($\Delta I = 0$) dipole transition. The DCO value for the 549-keV transition [Fig. 5(e)] supports it being dipole. The IPDCO values for the 265- and 549-keV transitions favor the magnetic character. The present measured DCO ratio value 0.47(6) for the 814-keV transition support the dipole character and $I^{\pi} = 14^{+}$ is assigned to the 4411-keV state. It is mentioned that the 265- and 814-keV transitions have been placed as $10^{+} \rightarrow 9^{+}$ and $11^{+} \rightarrow 9^{+}$, respectively, by Ghugre *et al.* [30], and $9^{-} \rightarrow 10^{+}$ and $10^{-} \rightarrow 10^{+}$, respectively, by Chattopadhyay *et al.* [31]. The DCO ratios for the 456- and 1136-keV transitions support these being dipole and quadrupole transitions, respectively, and the 5547-keV state is assigned $I^{\pi} = 16^{+}$. The present DCO ratio value 0.55(6) for the 1362-keV transition [Fig. 5(f)] indicates it is dipole. The transition is reported to be $E2$ both by Ghugre *et al.* [30] and Chattopadhyay *et al.* [31].

In the present level scheme, the 2484-keV state is assigned $I^{\pi} = 10^{+}$. The assignment of 11^{+} is unlikely as, being a weakly populated state, it cannot be yrast. The 413-keV transition with DCO ~0.81(14) is assigned to be $11^{+} \rightarrow 11^{+}$ magnetic dipole transition. The 994 (Q)–980 (Q)–1494 (Q)–456 (D) keV and 1407 (Q)–831 (Q)–1518 (Q)–167 (D) keV transition cascades are parallel and placed between the same 1624- and 5547-keV levels. It supports $I^{\pi} = 15^{+}$ for the 5380-keV level, and the quadrupole ($E2$) character for the 1518-keV transition. Overall, there is no indication of change of parity for the states in bands B1 and B5, and it is same as that of the 56-keV state.

The DCO ratio value for the 1152-keV transition [Fig. 5(g)] populating the 11^{+} level at 2618 keV indicate it to be a dipole transition of $M1$ type; therefore, the 3769-keV level is assigned $I^{\pi} = 12^{+}$. The $\Delta I = 0, 1, 2$ transitions from the states of bands B2 and B3 to those of band B1 compete with the intraband $M1$ transitions along with the crossover $E2$ transitions, and the interband $\Delta I = 0, 1$ transitions between states of bands B2 and B3. This supports $M1/E2$ nature for these transitions; i.e., parity of bands B2 and B3 is same as that of band B1. The 1611- and 1982-keV states are assigned $I^{\pi} = 6^{+}$ and 7^{+}, respectively. The spin assignments to the states in the coupled bands B2 and B3 are well supported by the DCO ratio values of the intraband transitions, and the interband transitions in bands B1, B2, and B3.

The measured DCO ratio value ~0.51(5) for the 463-keV transition support it being dipole. The IPDCO value and absence of any competing transition favor it to be an electric dipole $13^{-} \rightarrow 12^{+}$ transition. The transitions in the 792-1380-934-1348-1486 keV sequence has been assigned to be electric quadrupole on the basis of the present measured DCO and IPDCO values and the coupled structure established with the placement of new dipole transitions [Fig. 3(a)]. The higher-energy states in band B6 are assigned spin-parity values. These transitions have been reported to be $M1$ with the negative parity assigned to the involved states by Ghugre *et al.* [30] and $E2$ with the positive parity to the involved states by Chattopadhyay *et al.* [31].

The $I^{\pi} = 7^{+}$ level at 1982 keV decays to the 400-keV level by the 1066-516 keV cascade consisting of stretched dipole transitions. The 516-keV intense dipole transition with no other competing transition depopulating the 916-keV state is likely to be an electric one; i.e., it is associated with a parity change. Taking the 1066-keV transition also to be electric dipole, the spin-parities of the 916- and 400-keV levels are tentatively assigned to be (6^{-}) and (5^{+}), respectively. Both the 1290- and 1653-keV states are favorably assigned $I^{\pi} = 7^{+}$ on the basis of the usual $E2/M1$ multipolarity considerations for the linking transitions to the states with already assigned spins. The 1290-keV level decays to the (5^{+}) level at 400 keV by the 890-keV transition, which is also a crossover transition to the 374- and 516-keV transitions. The $I^{\pi} = (5^{+})$ assignment is favored for the 400-keV state as it is fed by the 497 keV transition from the 7^{+} state (band B1) and 605-605 keV transition cascade from the 6^{+} state at 1611 keV (band B2). The measured DCO ratio value 0.93(12) for the 605-keV transition depopulating the 6^{+} level at 1611 keV in band B2 indicate it to be a $\Delta I = 0$ dipole transition. The 1593- and 1879-keV states are tentatively assigned (7^{-}) and (8^{-}) on the basis of decay to the (6^{-}) state at 916 keV and the 7^{+} state at 1290 keV, and the 1879 keV is also being populated by 633-keV transition from the 9^{+} state.

IV. DISCUSSION

The level spacings and γ-ray intensities in bands B1–B6 in the present level scheme of ^{98}Rh (Fig. 1) suggest rotational excitations built on stable deformed minima in the potential-energy surfaces. The excitation energy vs spin plots for the bands observed in ^{98}Rh are shown in Fig. 6. Band B1 is the yrast one at lower spins and the coupled bands B2, B3, and B5 lie higher in excitation energy. Negative-parity band B6 becomes yrast in the higher spin region. The configuration assignment to the observed band structures can be inferred from the yrast level structures in the neighboring (odd-Z, even-N) isotopes and (even-Z, odd-N) isotones, respectively. The even-even ^{96}Ru core is known to be weakly deformed with β ~0.11 [9]. In the neighboring odd-A Rh isotopes, the lowest observed bands are based on the negative-parity

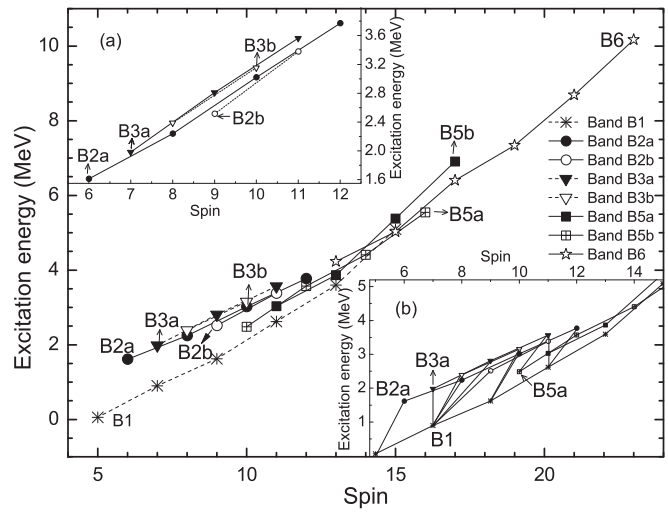

FIG. 6. Excitation energy vs spin plots for states in bands B1, B2, B3, B5, and B6 in ^{98}Rh. Inset shows the interband transitions from the states of bands B2 and B3 to the low-lying states of the yrast band B1 and band B5a. Inset shows the interband transitions from bands B2 and B3 to the low-lying states of yrast band B1 and band B5a.

$\pi p_{1/2}$ and the positive-parity $\pi g_{9/2}$ orbitals, and the energy difference between the respective bandheads, $1/2^-$ and ($7/2^+$ or $9/2^+$), is quite small, viz., +259, −64, −157, and −40 keV, in the odd-A $^{97-103}$Rh isotopes [16,17,30,55], respectively. In the neighboring the odd-A $^{97-101}$Ru isotopes [6,9,10], the $7/2^+$ bandhead of the $\nu g_{7/2}$ band lies ∼350 keV above the $5/2^+$ bandhead of the $\nu d_{5/2}$ band. The $\Delta I = 2$ decoupled bands based on the low-Ω $\nu h_{11/2}$ orbital are observed with the $11/2^-$ bandhead excitation energy increasing with decreasing neutron number, viz., the $\nu h_{11/2}$ bandheads lie at ∼2.25, 1.88, 1.07, and 0.53 MeV, in the odd-A $^{95-101}$Ru isotopes [6,9,10], respectively. Similar trends have been observed in the odd-A $^{97-103}$Pd isotopes and the odd-A $^{99-105}$Cd isotopes [50].

Further insight into the ^{98}Rh structure can be obtained by analyzing the rotational and electromagnetic properties of the observed bands (Fig. 1). The experimentally determined spins and level energies in ^{98}Rh have been transformed into the rotating frame of reference in accordance with the prescription of Bengtsson and Frauendorf [56]. The Routhians (energies in the rotating frame of nucleus) are obtained by subtracting a reference rotor with Harris parameters, $J_0 = 8.9\hbar^2$ MeV^{-1} and $J_1 = 15.7\hbar^4$ MeV^{-3} [57] from the measured level energies. The alignment (i_x) and Routhian (e') plots for these bands are shown in Figs. 7(a) and 7(b), respectively. The experimental $B(M1)/B(E2)$ values for the coupled bands B2, B3, B5, and B6 are plotted in Fig. 8. The observed alignments and relative positions of Routhians [Figs. 7(a) and 7(b)] for bands B1, B2, and B3 imply that these are rotational excitations built on the two-quasiparticle configurations involving the proton and neutron from the ($\pi p_{1/2}$, $f_{5/2}$, and $\pi g_{9/2}$) and ($\nu d_{5/2}$, $\nu g_{7/2}$, and $\nu h_{11/2}$) spaces, respectively.

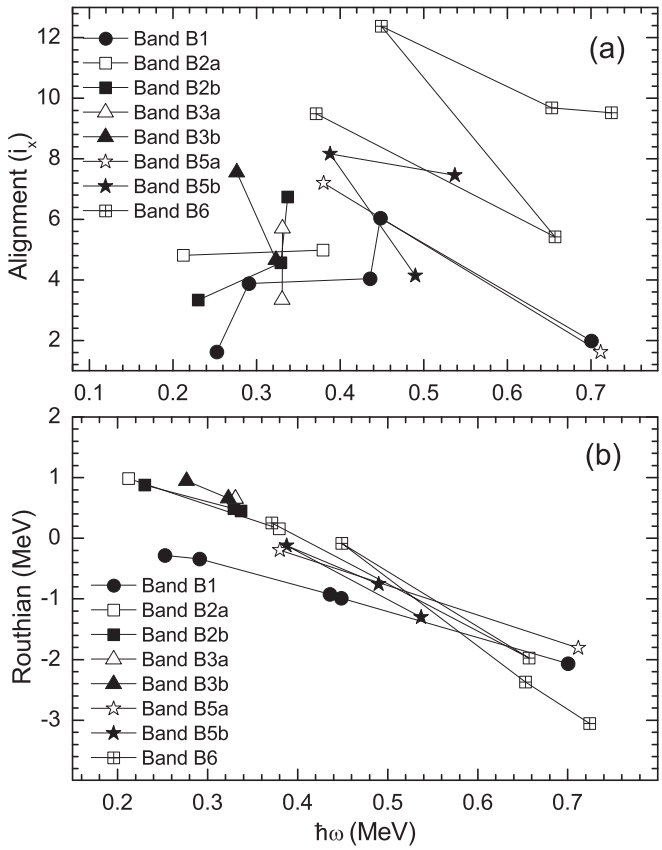

FIG. 7. Experimental (a) alignment (i_x) and (b) Routhian (e') plots for bands B1, B2, B3, B5, and B6 for ^{98}Rh. The values of Harris parameters used for the reference core are $J_0 = 8.9\hbar^2$ MeV^{-1} and $J_1 = 15.7\hbar^4$ MeV^{-3}.

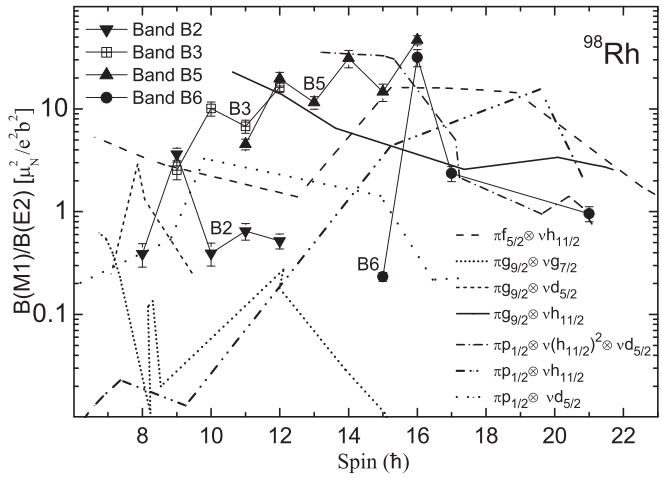

FIG. 8. The experimental $B(M1)/B(E2)$ values for the coupled bands B2, B3, B5, and B6 plotted as a function of spin. The plots are compared with those based on the TAC model calculations.

The configurations to the various observed bands are assigned on the basis of comparison of the rotational and electromagnetic properties with those calculated using the TAC shell model. The hybrid versions of TAC model calculations [33] have been performed for various possible configurations. In these calculations, the pairing parameters are chosen as 80% of the odd-even mass difference, i.e., $\Delta_\pi = 1.038$ MeV and $\Delta_\nu = 0.827$ MeV. The calculations have been performed for the $\pi g_{9/2} \otimes \nu h_{11/2}$ configuration in the ^{98}Rh nucleus, which is observed to be intensely populated in the heavier doubly odd $^{100-112}$Rh [14,18,47,48,54] isotopes. A self-consistent minimum is predicted around the quadrupole deformation parameter $(\epsilon_2) = 0.096$, the hexadecapole deformation parameter $(\epsilon_4) = 0$, the triaxiality parameter (γ) ∼29°, and an average tilt-angle (θ) ∼75°. The TAC model calculated angular momentum vs the rotational frequency plot for the $\pi g_{9/2} \otimes \nu h_{11/2}$ configuration is shown in Figs. 9(a)–9(c) along with the experimental ones for bands B1, B2, B3, B5, and B6. The plots for bands B5 and B6 match with the TAC calculated ones [Fig. 9(a)]. The predicted $B(M1)/B(E2)$ values for this configuration are large, ∼2–30 μ_N^2/e^2b^2, and exhibit decreasing trend with spin (Fig. 8). The values compare reasonably with those observed for bands B5 and B6. Systematics of the γ-transition energies and the excitation energies of states in the coupled $\pi g_{9/2} \otimes \nu h_{11/2}$ bands observed in the doubly odd $^{96,100-104}$Rh [14,18,48,49] and the $^{100-106}$Ag [50–52] nuclei, along with those in the coupled bands B2, B3, B5, and B6 observed in ^{98}Rh, are shown in Fig. 10. The plots for bands B2, B3, and B6 do not follow the systematics of the negative-parity $\pi g_{9/2} \otimes \nu h_{11/2}$ configuration. The configuration is also ruled out for band B1 due to its decoupled nature. The excitation energy plot for band B5 lies above that for the $\pi g_{9/2} \otimes \nu h_{11/2}$

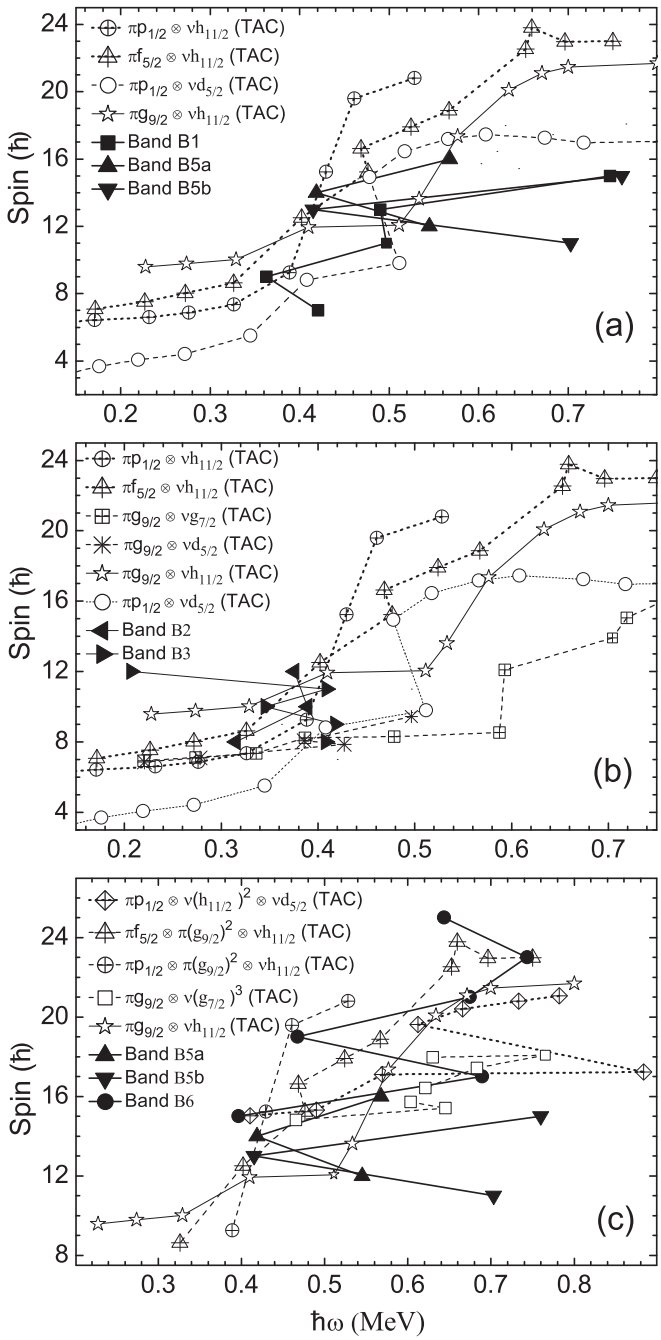

FIG. 9. The spin (I) vs frequency ($\hbar\omega$) plots for the observed (a) bands B1 and B5, (b) bands B2 and B3, and (c) bands B5 and B6. The results of the TAC calculations [33] based on different relevant configurations are also shown for comparison.

band of ^{96}Rh and the transition energies do not follow the systematics. The configuration is also not favored due to parity considerations.

The decoupled band B1 is the most intensely populated one. It shows average initial alignment of $\sim 4\hbar$. Among the various possible candidates, the $\pi p_{1/2} \otimes \nu h_{11/2}$ configuration involving low-Ω proton and neutron orbitals is expected to result in a band with no Ml transitions. The TAC model calculations [33] for the $\pi p_{1/2} \otimes \nu h_{11/2}$ configuration have been performed and a self-consistent minimum is predicted around the deformation parameters: $\epsilon_2 = 0.13, \epsilon_4 = 0, \gamma \sim 25^\circ$, and $(\theta) \sim 85^\circ$. The TAC model calculated angular momentum vs the rotational frequency plot for the $\pi p_{1/2} \otimes \nu h_{11/2}$ configuration is shown in Fig. 9(a) along with the experimental one for band B1. Keeping in mind that these parameters are sensitive function of the pairing gap parameter, theoretical calculations reasonably reproduce the experimental results. The predicted $B(M1)/B(E2)$ values for the $\pi p_{1/2} \otimes \nu h_{11/2}$ configuration are also very small, $\sim 0.01\ \mu_N^2/e^2b^2$. The observed band B1 is assigned the $\pi p_{1/2} \otimes \nu h_{11/2}$ configuration, which is the peaceful coupling case [51] of the two decoupled particles. The other positive-parity $\pi g_{9/2} \otimes \nu g_{7/2}/\nu d_{5/2}$ and the $\pi f_{5/2} \otimes \nu h_{11/2}$ configurations are also expected to result in the coupled structure (Fig. 8) as mentioned later in this section and hence these are not likely candidates for band B1.

Though only a few negative-parity states have been observed in doubly odd nuclei in this mass region, the $(\pi p_{1/2} \otimes \nu g_{7/2}/\nu d_{5/2})$ configurations that are responsible for the 2^- ground state of ^{102}Rh [18] are also considered for ^{98}Rh. The self-consistent TAC model calculations for the $\pi p_{1/2} \otimes \nu d_{5/2}$ configuration predict a self-consistent minimum around the deformation parameters $\epsilon_2 = 0.112$, $\epsilon_4 = -0.008$, $\gamma = 10.3^\circ$, and an average tilt angle $\theta \sim 76^\circ$. The TAC calculated angular momentum (I) vs rotational frequency ($\hbar\omega$) plot also compare reasonably with that for the observed band B1 [Fig. 9(a)]. However, the high $B(M1)/B(E2)$ predicted values ~ 0.4–$4\mu_N^2/e^2b^2$ in the observed range of frequencies (Fig. 8) do not favor this configuration for the observed decoupled band B1. The weakly populated coupled band B4 with few identified states is possibly based on the negative-parity $\pi p_{1/2} \otimes \nu d_{5/2}$ configuration. It is further added that the self-consistent TAC model calculations for the $\pi p_{1/2} \otimes \nu g_{7/2}$ configuration show no minimum to evolve into a rotational band.

The positive-parity coupled bands B2 and B3 show initial alignment ~ 3–$4\hbar$ [Fig. 7(a)] and small signature splitting $\lesssim 50$ keV [Fig. 7(b)]. The Routhian corresponding to the favored component of band B3 lies parallel and ~ 170 keV above that of band B2 [Fig. 7(b)]. Also, the excitation energy plots (Fig. 6) are parallel. There are considerable interband transitions in the two bands and these bands appear to be likely chiral partners. However, the experimental $B(M1)/B(E2)$ values for the states of band B3 are reasonably high $\sim 4\mu_N^2/e^2b^2$ and those of band B2 are relatively small $\sim 0.6(\mu_N^2/e^2b^2$ (Fig. 8). The intensities of the $M1$ interband transitions from the states of band B3 to band B2 are also comparable to those of the intraband transitions, and the $B(M1)_{in}/B(M1)_{out}$ values for the 10^+ and 11^+ states in band B3 are $\sim 5\mu_N^2/e^2b^2$, respectively. Both the TAC model predicted angular momentum (I) vs rotational frequency ($\hbar\omega$) plots [Fig. 9(b)] and the $B(M1)/B(E2)$ values (Fig. 8) for the $\pi g_{9/2} \otimes \nu h_{11/2}$ configuration responsible for chiral bands [12–15] in this mass region differ significantly from the experimental ones for bands B2 and B3.

The other likely candidates for bands B2 and B3 are the $\pi g_{9/2} \otimes \nu g_{7/2}$ and $\pi g_{9/2} \otimes \nu d_{5/2}$ configurations, and the TAC model calculations exhibit self-consistent minimum around the sets of deformation parameters $(\epsilon_2 = 0.09, \epsilon_4 = 0, \gamma = -4^\circ$, and $\theta \sim 70^\circ)$ and $(\epsilon_2 = 0.10, \epsilon_4 = -0.005, \gamma = 0^\circ,$

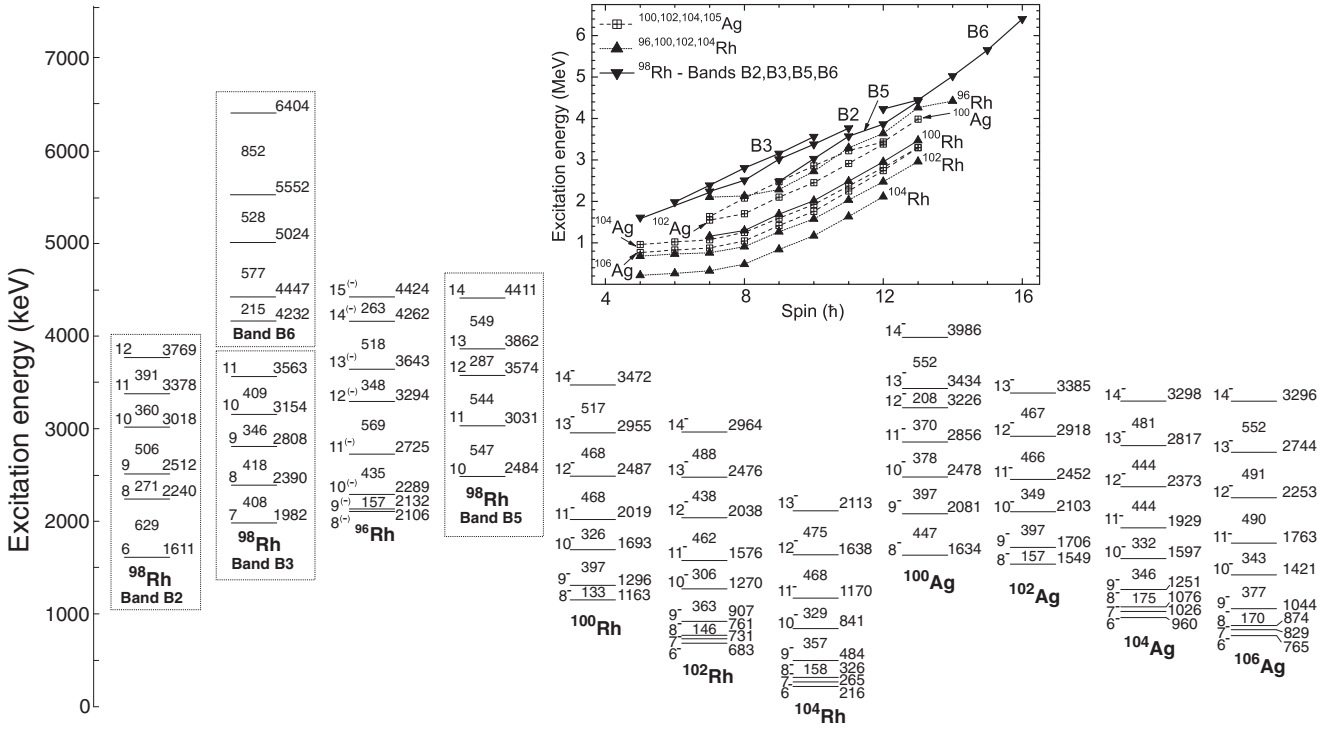

FIG. 10. Systematics of the excitation energies of states and transition energies in the $\pi g_{9/2} \otimes \nu h_{11/2}$ bands observed in the odd-odd $^{96-104}$Rh [14,18,48,49] and $^{100-106}$Ag [50–52] isotopes. Inset also shows the excitation energy plot. The coupled bands B2, B3, B5, and B6 observed in ^{98}Rh from the present level scheme are also included for comparison.

and $\theta \sim 65^\circ$), respectively. The angular momentum (I) vs rotational frequency ($\hbar\omega$) plots for the $\pi g_{9/2} \otimes \nu g_{7/2}$ and $\pi g_{9/2} \otimes \nu d_{5/2}$ configurations are compared with bands B2 and B3 in Fig. 9(b). Neither of these configurations generate angular momentum up to ~0.5 MeV, i.e., over the observed range of frequencies.

Bands B2 and B3 also decay to the states of band B1 ($\pi p_{1/2} \otimes \nu h_{11/2}$) through the $\Delta I = 0, 1, 2$ transitions. In view of this, the $\pi f_{5/2} \otimes \nu h_{11/2}$ configuration is also considered for bands B2 and B3. The negative-parity $\pi f_{5/2}$ orbital lies close to the $\pi p_{1/2}$ and is expected to result in a coupled band. The TAC model calculations for the $\pi f_{5/2} \otimes \nu h_{11/2}$ configuration give a self-consistent minimum at $\epsilon_2 = 0.14$, $\epsilon_4 = -0.02$, $\gamma = 9^\circ$, and an average tilt angle $\theta \sim 75^\circ$. The results of the calculations of angular momentum (I) vs rotational frequency ($\hbar\omega$) together with the observed bands B2 and B3 are shown in Fig. 9(a). The predicted $B(M1)/B(E2)$ values compare reasonably with the observed ones for band B3. The theoretical results for the $\pi f_{5/2} \otimes \nu h_{11/2}$ configuration compare reasonably well with the experimental data for band B3. Band B3 is assigned the two-quasiparticle $\pi f_{5/2} \otimes \nu h_{11/2}$ configuration.

The angular momentum vs frequency plot for the $\pi f_{5/2} \otimes \nu h_{11/2}$ configuration follow closely to the one for the $\pi p_{1/2} \otimes \nu h_{11/2}$ configuration. However, the $B(M1)/B(E2)$ values for the $\pi f_{5/2} \otimes \nu h_{11/2}$ configuration are high, ~3–4μ_N^2/e^2b^2, implying a coupled nature with strong $M1$ transitions, while no $M1$ transitions are predicted for the $\pi p_{1/2} \otimes \nu h_{11/2}$ configuration. The observed parallelism in the excitation energy plots (Fig. 6) for the states of bands B2 and B3, along with considerable interband $M1$ transitions, and also decay to the states of band B1, suggest similar configurations for these bands. For a fully aligned (doubly decoupled) $\pi p_{1/2} \otimes \nu h_{11/2}$ configuration no $M1$ transitions are expected. However, admixtures from the $p_{1/2}$ and $f_{5/2}$ parentage are likely to be present in band B2, increasing the effective g factor and the quasiparticle angular momentum projection along the symmetry axis (K). The mixing can result in small observed $B(M1)/B(E2)$ ratio ~0.4μ_N^2/e^2b^2 for band B2. It may be added that the angular momentum (I) vs rotational frequency ($\hbar\omega$) plot for the $\pi p_{1/2} \otimes \nu d_{5/2}$ negative-parity configuration also agrees with the observed band B2, and the $B(M1)/B(E2)$ ratio values are reasonably reproduced. However, the configuration is unlikely for band B2 on the basis of the parity considerations.

Band B5 observed in continuation to band B1 is coupled one. The states in the excited band B5 have the same positive parity as that for band B1 and decay to band B1 through the 413-keV ($11^+ \rightarrow 11^+$), 265-keV ($13^+ \rightarrow 13^+$) transitions, and the 860-keV ($10^+ \rightarrow 9^+$), 957-keV ($12^+ \rightarrow 11^+$), 814-keV ($14^+ \rightarrow 13^+$), and 456-keV ($16^+ \rightarrow 15^+$) transitions. The expected 289-keV ($15^+ \rightarrow 15^+$) transition is not observed. Band B1 decays to the states of band B5 through the 134-keV ($11^+ \rightarrow 10^+$) and 680-keV ($15^+ \rightarrow 14^+$) transitions. Band B5 shows small signature splitting ~50 keV at $\hbar\omega = 0.30$ MeV [Fig. 7(b)]. The $B(M1)/B(E2)$ values for the states are high, ~10–50μ_N^2/e^2b^2 [(ig. 8). The negative-parity $\pi g_{9/2} \otimes \nu h_{11/2}$ configuration for band B5 has been ruled out as discussed earlier. The positive-parity four-quasiparticle configurations, viz., $\pi p_{1/2}/f_{5/2} \otimes \pi(g_{9/2})^2 \otimes \nu h_{11/2}$, $\pi p_{1/2}/f_{5/2} \otimes \pi(g_{7/2})^2 \otimes \nu h_{11/2}$, and $\pi g_{9/2} \otimes \pi(g_{7/2})^3$, are the expected

candidates for band B5. The TAC model calculations for the $\pi g_{9/2} \otimes \nu(g_{7/2})^3$ configuration give self-consistent minimum corresponding to the deformation parameters, $\epsilon_2 = 0.100$, $\epsilon_4 = -0.005$, $\gamma = 0.0^\circ$, and $\theta \sim 75^\circ$. The experimental spin vs frequency plot for band B5 does not exhibit good agreement with the TAC model predictions for this configuration [Fig. 9(c)] and also it gives small $B(M1)/B(E2)$ values $\sim 0.5\mu_N^2/e^2b^2$. The spin vs frequency plot for band B5 exhibits good agreement with the TAC model predictions for the $\pi p_{1/2} \otimes \nu h_{11/2}$ [Fig. 9(a)] and $\pi f_{5/2} \otimes \nu h_{11/2}$ [Fig. 9(c)] configurations after alignment of the $\pi g_{9/2}$ pair. It is worth noting that the band based on these configurations shows a jump in the TAC predicted $B(M1)/B(E2)$ values to $\sim 20\mu_N^2/e^2b^2$ (Fig. 8) after alignment of the $\pi g_{9/2}$ pair. The presence of the $g_{9/2}$ quasiprotons leads to $M1$ transitions stronger by an order of magnitude. A band based on such configurations has been observed in ^{108}Ag (Fig. 4 of Ref. [53]) with large $B(M1)/B(E2)$ values. Band B5 is in continuation of band B1 and assigned the $\pi p_{1/2}/f_{5/2} \otimes \pi(g_{9/2})^2 \otimes \nu h_{11/2}$ configuration.

The negative-parity band B6 is built on the $I^\pi = 13^-$ state at 4231 keV. Speculations regarding the structure of band B6 include rotational excitations built on the $\nu h_{11/2}$ pair contributing high alignment. The TAC model calculations have been performed for the $\pi p_{1/2}/f_{5/2} \otimes \nu(h_{11/2})^2 \otimes \nu d_{5/2}$ configuration and the optimized parameters come out to be $\epsilon_2 = 0.17$, $\epsilon_4 = -0.008$, $\gamma = 37.5^\circ$, and $\theta \sim 80^\circ$. The $\pi p_{1/2} \otimes \nu(h_{11/2})^2 \otimes \nu d_{5/2}$ configuration exhibits overall good agreement with the experimental data for the observed band B6. The bandhead spin 13^- is also reproduced for the $\pi p_{1/2} \otimes \nu(h_{11/2})^2 \otimes \nu d_{5/2}$ configuration. The $B(M1)/B(E2)$ values are well reproduced (Fig. 8).

V. CONCLUSIONS

The level scheme of the doubly odd ^{98}Rh nucleus has been studied using in-beam γ-ray spectroscopic techniques following its population in the ^{75}As(^{28}Si,$2p3n$) fusion-evaporation reaction. The resulting level scheme in ^{98}Rh consists of six bands established up to spin $\sim 23\hbar$. The earlier reported level schemes have been substantial modified. About 90 new transitions have been included. It is concluded that the 842-726-994-980-265 keV γ-transition cascade in ^{98}Rh is not directly based on the ground state ($T_{1/2} = 8.7$ min) as reported earlier [30,31]. It feeds the new proposed level at 56 keV. Further experiments are warranted to establish the lower part of the level scheme and study the new proposed isomeric states at 48 and 56 keV. In the present level scheme of ^{98}Rh, the spin-parity assignments are relative and have been done on the assumption of usual multipolarity for the decay transitions, DCO ratio, and polarization measurements. The absolute spin-parity assignments are not possible in view of the unestablished decay of the identified low-lying states. Tilted-axis cranking (TAC) shell-model calculations have been performed to interpret the level scheme of ^{98}Rh and assign configurations to various observed bands. The identified bands in the level scheme have been interpreted in terms of the rotational bands based on the $\pi p_{1/2} \otimes \nu h_{11/2}$ and $\pi f_{5/2} \otimes \nu h_{11/2}$, and the admixture, $\pi p_{1/2} \otimes \pi(g_{9/2})^2 \otimes \nu h_{11/2}$, and $\pi p_{1/2} \otimes \nu(h_{11/2})^2 \otimes \nu d_{5/2}$ configurations. The negative-parity band based on the $\pi g_{9/2} \otimes \nu h_{11/2}$ configuration is not observed in the more neutron-deficient ^{98}Rh isotope, which is observed to be yrast in the heavier doubly odd $^{100-112}$Rh isotopes. The bandhead spin values deduced for the assigned configurations from TAC model calculations support the integrity of the spin-parity assignments in ^{98}Rh.

ACKNOWLEDGMENTS

The authors thank the operational staff of the 15UD Pelletron at IUAC and the INGA Collaboration. The authors also thank the Department of Science and Technology, Government of India for providing funding for the INGA project (No. IR/S2/PF-03/2003-I). Financial support from UGC, New Delhi, under the Center of Advanced Study Funds is duly acknowledged.

[1] G. García Bermúdez and M. A. Cardona, Phys. Rev. C **64**, 034311 (2001).
[2] J. Timár *et al.*, Acta Phys. Pol. B **33**, 493 (2002).
[3] K. Hara and Y. Sun, Nucl. Phys. A **537**, 77 (1992).
[4] V. I. Dimitrov, S. Frauendorf, and F. Dönau, Phys. Rev. Lett. **84**, 5732 (2000).
[5] K. Higashiyama, N. Yoshinaga, and K. Tanabe, Phys. Rev. C **72**, 024315 (2005).
[6] A. D. Yamamoto *et al.*, Phys. Rev. C **66**, 024302 (2002).
[7] S. Lalkovski *et al.*, Phys. Rev. C **71**, 034318 (2005).
[8] N. V. Zamfir and R. F. Casten, Phys. Lett. B **260**, 265 (1991).
[9] B. Kharraja *et al.*, Phys. Rev. C **57**, 83 (1998).
[10] J. Timár *et al.*, Phys. Rev. C **62**, 044317 (2000).
[11] J. Srebrny *et al.*, Nucl. Phys. A **766**, 25 (2006).
[12] J. Meng and S. Q. Zhang, J. Phys. G **37**, 064025 (2010).
[13] P. Joshi *et al.*, Eur. Phys. J. A **24**, 23 (2005).
[14] C. Vaman, D. B. Fossan, T. Koike, K. Starosta, I. Y. Lee, and A. O. Macchiavelli, Phys. Rev. Lett. **92**, 032501 (2004).
[15] P. Joshi *et al.*, Phys. Lett. B **595**, 135 (2004).
[16] M. Sugawara *et al.*, Phys. Rev. C **87**, 064319 (2013).
[17] J. Timár *et al.*, Eur. Phys. J. A **4**, 11 (1999).
[18] J. Gizon *et al.*, Phys. Rev. C **59**, R570 (1999).
[19] J. Cederkäll *et al.*, Z. Phys. A **359**, 227 (1997).
[20] S. Sihotra, Z. Naik, S. Kumar, K. Singh, J. Goswamy, N. Singh, R. Kumar, R. P. Singh, S. Muralithar, R. K. Bhowmik, R. Palit, and D. Mehta, Phys. Rev. C **83**, 024313 (2011).
[21] J. Gizon *et al.*, Phys. Lett. B **410**, 95 (1997).
[22] B. M. Nyakó *et al.*, Phys. Rev. C **60**, 024307 (1999).
[23] J. Cederkäll *et al.*, Eur. Phys. J. A **1**, 7 (1998).
[24] D. Sohler *et al.*, Eur. Phys. J. A **16**, 171 (2003).
[25] A. V. Afanasjev, D. B. Fossan, G. J. Lane, and I. Ragnarsson, Phys. Rep. **322**, 1 (1999).
[26] M. Gasior, A. W. Potempa, H. Roth, and J. Sieniawski, Acta Phys. Pol. B **3**, 2 (1972).
[27] B. Singh and Z.g. Hu, Nucl. Data Sheets **98**, 335 (2003).
[28] J. Ashkenazi, E. Friedman, D. Nir, and J. Zioni, Nucl. Phys. A **158**, 146 (1970).

[29] M. Behar, A. M. J. Ferrero, A. Filevich, and A. O. Macchiavelli, Z. Phys. A **314**, 111 (1983).
[30] S. S. Ghugre *et al*., Phys. Rev. C **58**, 3243 (1998).
[31] S. Chattopadhyay, A. Mukherjee, U. Datta Pramanik, A. Goswami, S. Bhattacharya, B. Dasmahapatra, S. Sen, H. C. Jain, and P. K. Joshi, Phys. Rev. C **57**, R471 (1998).
[32] S. Muralithar *et al*., Nucl. Instr. Meth. A **622**, 281 (2010).
[33] S. Frauendorf and J. Meng, Nucl. Phys. A **617**, 131 (1997).
[34] Surender Kumar, S. Sihotra, K. Singh, J. Goswamy, N. Singh, R. Palit, S. Muralithar, R. Kumar, R. P. Singh, R. K. Bhowmik, and D. Mehta, Proc. of DAE-BRNS Symp. on Nucl. Phys. **55**, 44 (2010).
[35] S. Kumar, S. Sihotra, K. Singh, V. Singh, J. Goswami, N. Singh, R. Palit, S. Muralithar, R. Kumar, R. P. Singh, R. K. Bhowmik, S. K. Ghorui, C. R. Praharaj, and D. Mehta, AIP Conf. Proc. **1524**, 127 (2013).
[36] G. K. Mehta and A. P. Patro, Nucl. Instr. Meth. A **268**, 334 (1988).
[37] D. Kanjilal *et al*., Nucl. Instr. Meth. A **328**, 97 (1993).
[38] D. Rudolph *et al*., Phys. Rev. C **65**, 034305 (2002).
[39] T. Andersson *et al*., Eur. Phys. J. A **6**, 5 (1999).
[40] M. Hausmann *et al*., Phys. Rev. C **68**, 024309 (2003).
[41] R. K. Bhowmik, S. Muralithar, and R. P. Singh, Proc. of DAE-BRNS Symp. on Nucl. Phys. **44B**, 422 (2001).
[42] D. C. Radford, Nucl. Instr. Meth. A **361**, 297 (1995); **361**, 306 (1995).
[43] A. Krämer-Flecken, T. Morek, R. M. Lieder, W. Gast, G. Hebbinghaus, H. M. Jäger, and W. Urban, Nucl. Instr. Meth. A **275**, 333 (1989).
[44] K. Starosta, T. Morek, Ch. Droste, S. G. Rohoziski, J. Srebrny, A. Wierzchucka, M. Bergström, B. Herskind, E. Melby, T. Czosnyka, and P. J. Napiorkowski, Nucl. Instr. Meth. A **423**, 16 (1999).
[45] A. H. W. Aten, Jr. and J. C. Kapteyn, Physica (Amsterdam) **32**, 989 (1966).
[46] V. Banerjee, A. Banerjee, G. S. N. Murthy, R. P. Sharma, S. K. Pardha Saradhi, and A. Chakrabarti, Phys. Rev. C **49**, 1221 (1994).
[47] R. Duffait, A. Charvet, K. Deneffe, R. Beraud, A. Emsallem, M. Meyer, and T. Ollivier, Nucl. Phys. A **454**, 143 (1986).
[48] A. Gizon *et al*., Eur. Phys. J. A **2**, 325 (1998).
[49] W. F. Piel, Jr., D. B. Fossan, R. Ma, E. S. Paul, N. Xu, and J. B. McGrory, Phys. Rev. C **41**, 1223 (1990).
[50] R. Alfier, D. Alber, H. Grawe, H. Kluge, K. H. Maier, R. Schubart, D. B. Fossan, and W. F. Piel, Z. Phys. A **355**, 135 (1996).
[51] J. Tréherne *et al*., Phys. Rev. **27**, 166 (1983).
[52] C. Y. He *et al*., Phys. Rev. C **81**, 057301 (2010).
[53] F. R. Espinoza-Quiñones, E. W. Cybulska, L. G. R. Emediato, C. L. Lima, N. H. Medina, J. R. B. Oliveira, M. N. Rao, R. V. Ribas, M. A. Rizzutto, W. A. Seale, and C. Tenreiro, Phys. Rev. C **52**, 104 (1995).
[54] N. Fotiades, J. A. Cizewski, R. Krucken, D. P. McNabb, J. A. Becker, L. A. Bernstein, W. Younes, R. M. Clark, P. Fallon, I. Y. Lee, and A. O. Macchiavelli, Phys. Rev. C **67**, 064304 (2003).
[55] H. Dejbakhsh, R. P. Schmitt, and G. Mouchaty, Phys. Rev. C **37**, 621 (1988).
[56] R. Bengtsson and S. Frauendorf, Nucl. Phys. A **327**, 139 (1979).
[57] R. P. Singh, R. K. Bhowmik, S. S. Ghugre, and S. B. Patel, Eur. Phys. J. A **7**, 35 (2000).